Exp. Theo. NANOTECHNOLOGY 7 (2023) 131 - 142 https://doi.org/10.56053/7.3.131

Analysis of flakes-based BiOI nanostructure

*W. Antoine, K. Kennedy**

Department of Materials Science, University of Windsor, Windsor, Ontario, N9B 3P4 Canada
*) Email: ken@uwindsor.ca

Received 17/12/2022, *Accepted*, 30/1/2023, *Published* 15/4/2023

This article reports the comprehensive details of structure, morphology, mechanical, thermal, and optical details of BiOI material and film, combining both experimental and first-principle calculations. The structure, morphology, atomic concentration, and optical properties have been investigated via XRD, SEM, EDX, and UV-vis analysis. Moreover, the first-principle calculations have been performed applying the plane-wave pseudopotential based density functional theory (DFT) to investigate the structural aspects, mechanical behaviors, thermal, and optical characteristics of the prepared BiOI compound. The calculated lattice constants reasonably agree with its experimental values. BiOI's mechanical stability requirement is perfectly fulfilled by the derived elastic constants. This BiOI compound could be utilized as a thermal barrier coating (TBC) material because of the calculated Debye temperature and minimum thermal conductivity. Furthermore, crucial optical factors such as absorption coefficient, dielectric constants, photoconductivity, loss function, refractive index, and reflectivity are studied and described in order to maximize the effectiveness of BiOI applications.

Keywords: Experimental-synthesis-BiOI; Dip-SILAR process; Structural.

1. INTRODUCTION

BiOI emerges as a trustworthy appreciative in the areas of material science for a variety of reasons, such as higher stability, low cost, and prospective visible light active photo-catalytic (VLAP) utilization for wastewater treatment features [1], especially after the development of BiOX structure (X: Cl, Br, I) in 1935. BiOI has a tetragonal structure and has a good ability to separate the photo-produced electron-hole (e-/h+) pairs with low generation cost [2]. Furthermore, BiOI's broad visible spectral range encourages us to think of it as an absorber or a

prospective photo-catalytic for photovoltaic uses [3]. The BiOI thin film is now being produced in a variety of ways by scientists throughout the world. Chemical Bath Deposition (CBD), sol-gel method, spin coating, and Dual-port ultrasonic spray pyrolysis technique, are among the most extensively applied synthesis methods in the literature. Thin BiOI films, on the other hand, are produced utilizing the successive ionic layer adsorption and reaction (SILAR) technique. In our experiment, the BiOI has been prepared via the dip-SILAR technique; based on the previously reported articles, this method can produce uniform film compare to others. It is possible to generate various structures of BiOI with various morphologies, such as nano-plates, BiOI microspheres, and flaky BiOI structure, using various synthesis techniques. These structures of BiOI were developed through a wet chemical method using $Bi(NO3)3.5H2O$ or $NaBiO3.2H2O$. On the other hand, earlier research has shown that single-crystal nano-sheet BiOI can also be produced from the $BiI3$ powder using the annealing treatment [4]. The band-gap of BiOI material regulates its photocatalytic features directly, but the band-gap of BiOX is logically determined by the atomic number of halogens in BiOX. The efficient band-gap of BiOI is 1.89 eV, according to various research studies, which was verified by the threshold wavelength of 650 nm. However, the photocatalytic activity is improved by the efficient band-gap. The narrow band-gap of BiOI, on the other hand, is responsible for the increased recombination rate of photo-generated electron-hole pairs. As a result, it is pointing to a degradation in the quantum efficiency of BiOI films [5]. These issues need more investigations on the BiOI films. All the reported research articles highlighted the photovoltaic and optical properties of BiOI material. However, no research has been published that combines experimental and first-principles calculations to provide additional insights into the emerging BiOI material. In this research article, the structure, morphology, mechanical, thermal, and optical properties of BiOI have been briefly explored and illustrated by combining both experimental and first-principles schemes.

2. EXPERIMENTAL

In the experiment, a fluorine-doped tin oxide (FTO) glass substrate BiOI was deposited on top of a 2 cm x 2 cm glass substrate. The FTO glass substrate had previously been cleaned with acetone, ethanol, and $N2$ gas. Furthermore, $Bi(NO3)3.5H2O$ and KI (purchased from Nacalai Tesque, Inc. Kyoto, Japan) were employed as cation and anion sources, respectively, throughout the BiOI deposition procedure. In our experiment, without any further purification all solvents were used, and for solution making, ultrapure water was acquired from Milli-Q direct water purification system (specification: 18.2 MΩ-cm (resistivity) and 25^{o}C (temperature)). Here, the deposition process has been conducted via the dip-SILAR process. The details of the dip-SILAR process can be found in previously reported articles [6]. In the structural investigation, The Rigaku SmartLab X-ray diffractometer with Cu-Kβ filter (45kV/200mA) was adopted to acquire X-ray diffraction (XRD) patterns of the processed specimens at room temperature. The scan rate of 2θ was 12°/ min and recorded over the range of 8-60°. Henceforth, to analyze the morphological and optical investigation, the reflectance R(λ), transmittance T (λ) and SEM image were measured through UV-Visible NIR spectroscopy (JASCO 670 UV) and scanning electron microscopy (SEM, JSM-6510).

According to our experimental study, the compound BiOI is crystallized in tetragonal crystal structure with the space group $P4/nmm$ (No. 129). The determined lattice constants are a = b = 3.97, and c = 9.22 Å [7]. In the present study, the first-principles calculations were accomplished employing the Cambridge Serial Total Energy Package (CASTEP) [36]in the framework of density functional

theory (DFT), based on the pseudo-potential plane-wave (PP-PW) total energy calculation. The Vanderbilt-type ultrasoft pseudopotential was selected to accommodate electron-ion interactions [8]. The exchange-correlation potential was characterized using the Perdew-Burke-Ernzerhof (PBE) and the Generalized Gradient Approximation (GGA) [9]. To assure convergence, cut-off energy of 500 eV was chosen. The k-points of 14×14×6 sample integration, which were adjusted to ultrafine grade over the first Brillouin zone, were employed with the Monkhorst-Pack technique [10]. The internal atomic coordinates and lattice constants were calculated adopting the Broyden–Fletcher–Goldfarb–Shanno (BFGS) technique. During the structural optimization procedure, all lattice parameters and atomic places were relaxed. All computations are done at zero pressure, which allows all lattice constants, atomic sites, and angles to relax completely. Maximum ionic displacement within 5×10^{-4}Å, maximum stress within 0.02 GPa, total energy difference per atom within 5×10^{-6} eV, and maximum ionic Hellmann-Feynman force within 0.01 eV are the tolerances chosen for optimizing the system geometry. Based on the aforementioned parameters, the mechanical and optical characteristics were determined. The elastic moduli and elastic constants were also determined adopting the "stress-strain" approach. The elastic anisotropy was calculated using the elastic constants by employing open source online ELATE program.

3. RESULTS AND DISCUSSIONS

In our study to understand the structural behavior of dip-SILAR prepared BiOI film at 30cycles, the XRD pattern has been recorded and depicted in Figure 1. In Figure 1, some sharp peaks have been appeared at the position of 9.6 º (001), 29.7 º (102), 31.7 º (110), 36.8 º (013), 39.2 º (004), 45.5 º (200), 51.2 º (114), and 55 º (122). Meanwhile, all the recorded peaks are for BiOI, which we have confirmed via Joint Committee on Powder Diffraction Standards (JCPDS) card No. 00-073-2062. Simultaneously, it demonstrates a reasonable degree of consistency with earlier articles. Among the all peaks the intensity of the (102) plane is higher and according to previously reported article we can claim that it the most favorable plane for BiOI. Moreover, the crystallite size has been calculated using the Scherrer’s formula, which is around 15.9 nm.

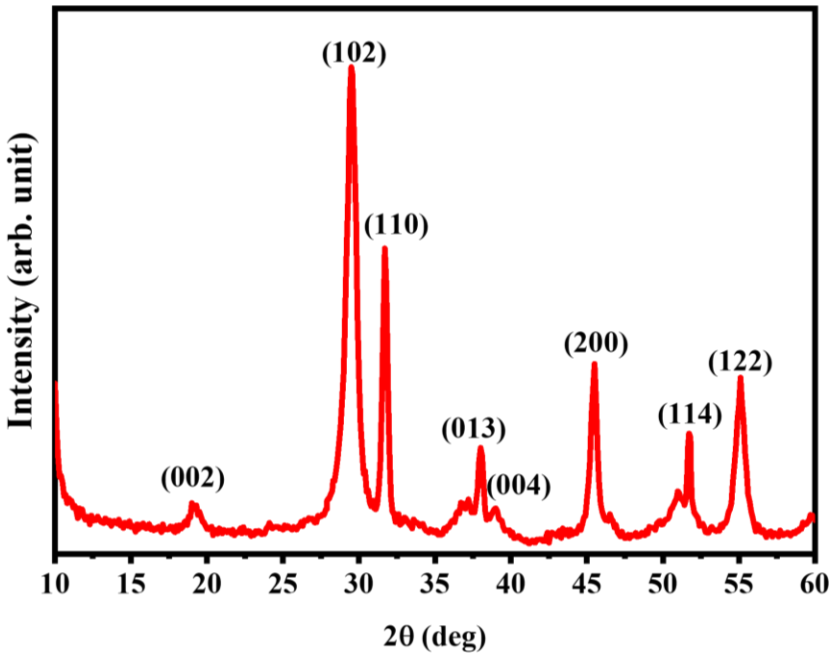

Figure 1 XRD pattern of dip-SILAR prepared BiOI.

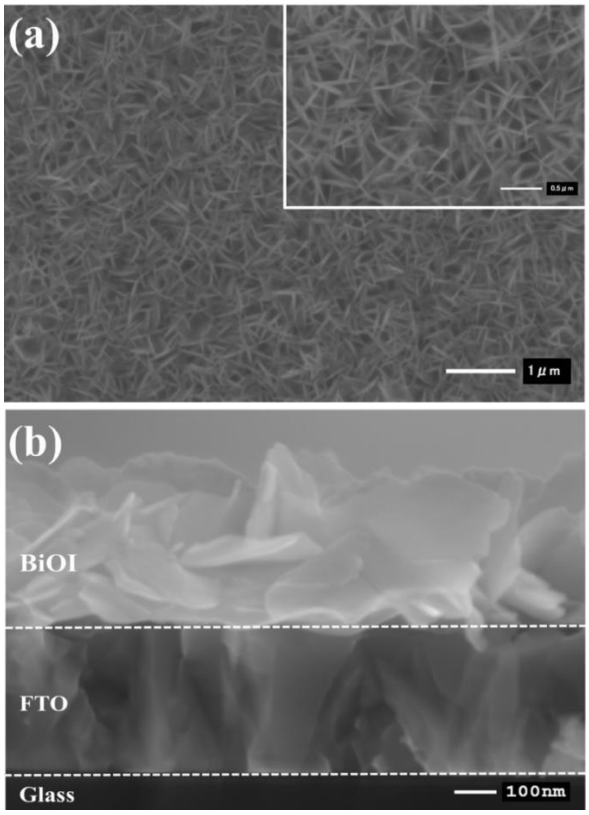

Figure 2 Morphological view of dip-SILAR prepared BiOI (a) surface view (b) cross-sectional view.

To understand the morphology of the prepared BiOI films, the SEM image has been captured and shown in Figure 2a, which shows a flaky structure of dip-SILAR prepared BiOI and the flakes are connected with each other. Moreover, a cross-sectional FESEM image presented in Figure 2b has been captured to understand how BiOI is connected with the FTO. The flakes are almost perpendicularly connected with the FTO. The measured thickness of the BiOI film is around 500 nm and the average flake size is around 350~400 nm. Our experiment is clearly hinting that flakes based uniform BiOI film can be produced via dip-SILAR process (see Figure 2a).
At the same time the atomic concentration of the prepared BiOI film has been measured and presented in Figure 3. The atomic concentration ratio of 'Bi' and 'I' is around 1: 1, indicating that the dip-SILAR process is capable of maintaining balance distribution of atoms. However, in terms of photovoltaic properties it is still not up to the mark, despite having decent properties. As a result, in order to progress to the next stage of photovoltaic application, further research into this emerging material is needed.

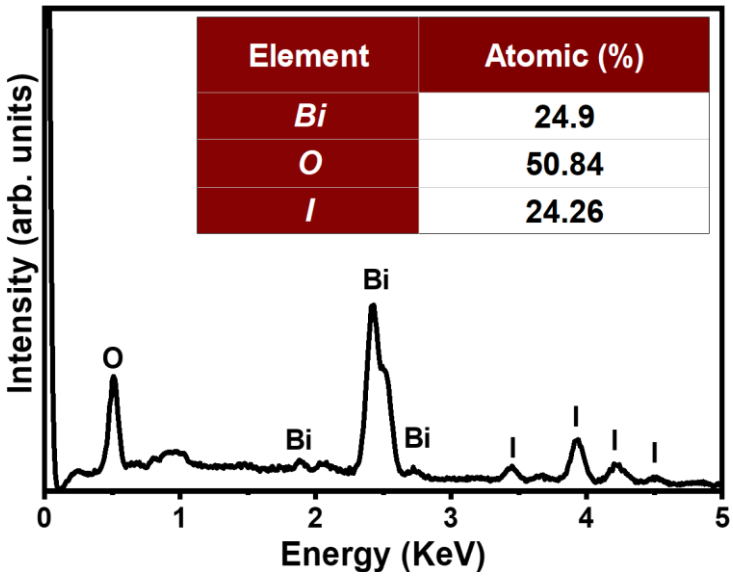

Figure 3 Atomic concentration of dip-SILAR prepared BiOI.

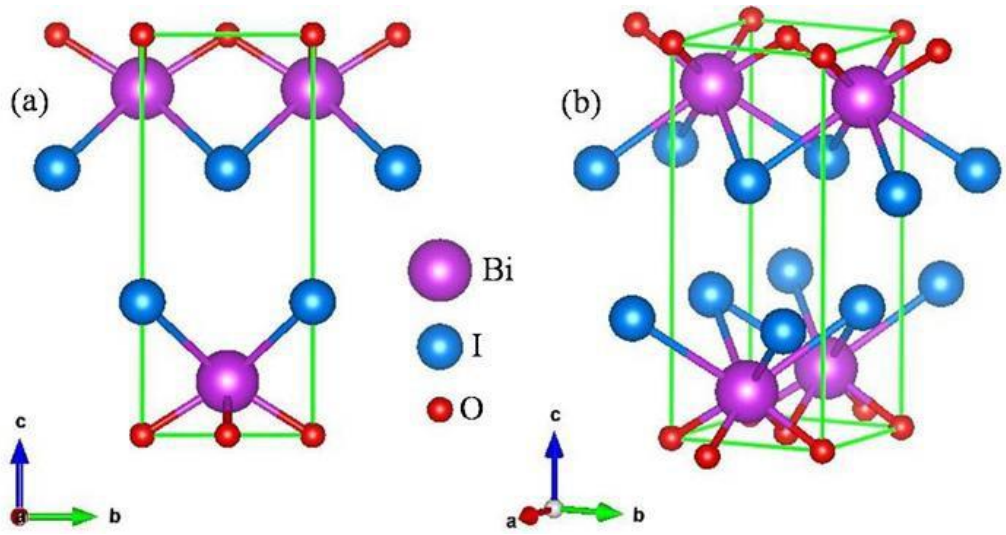

Figure 4 The conventional optimized crystal structure of tetragonal BiOI, (a) 2D and (b) 3D image.

The BiOI was formed in a tetragonal structure with the space group of *P*4/*nmm* (No. 129). The equilibrium crystal structure was first constructed using the experimentally determined lattice constants $a = b = 3.97$ and $c = 9.22$, as well as the Wyckoff positions Bi (0, 0.5, 0.1294), O (0, 0, 0), and I (0, 0.5, 0.6760). Figure 4 shows the conventional cell of tetragonal BiOI after optimization. We have calculated the ground state structural parameters, like lattice constants (*a*) and unit cell volume (V), by reducing the overall energy and force convergence at zero pressure and temperature. The elastic constants are used to explain the bonding properties, solid stability, ductile-brittle behavior, machinability, and elasticity of solid materials under equilibrium conditions. The elastic constants of tetragonal material must meet the Born stability requirements to become a stable system.

$C_{11} > 0, C_{33} > 0, C_{44} > 0, C_{66} > 0$

$C_{11} - C_{12} > 0, C_{11} + C_{33} - 2C_{13} > 0$ (1)

$2(C_{11} + C_{12}) + C_{33} + 4C_{13} > 0$

The elastic constants of BiOI completely justified the aforementioned conditions, ensuring its mechanical stability. Since, the value of C_{11} was greater than that of C_{33}, the bonding energy was significantly higher in the [010] and [100] directions than in the [001]. As a result, the compressibility along [001] was weaker than along [100]. Shear deformation happened more conveniently in the [001] direction than along the [010] direction because C_{44} is smaller than C_{66}. However, $C_{11} + C_{12} > C_{33}$, the bonding in the (001) plane and the elastic tensile modulus were elastically more stiff and higher along the c-axis. Applying the well-known Voigt-Reuss-Hill approximations, the shear modulus (G) and bulk modulus (B) were estimated.

$$B_V = \frac{2}{9}(C_{11} + C_{12} + 2\,C_{13} + \frac{C_{12}}{2}) \quad (2)$$

$$B_R = \frac{C^2}{M} \quad (3)$$

Where $C^2 = (C_{11} + C_{12})C_{33} - 2C^2_{13})$ and $M = (C_{11} + C_{12} + 2C_{33} - 4C_{13})$

$$G_V = \frac{(M + 3C_{11} - 3C_{12} + 12C_{44} + 6\,C_{66})}{30} \quad (4)$$

$$G_R = \frac{15}{\left(\frac{18B_V}{C^2} + \frac{6}{(C_{11}-C_{12})} + \frac{6}{C_{44}} + \frac{3}{3C_{44}}\right)} \quad (5)$$

$$B = \frac{1}{2}(B_V + B_R);\ G = \frac{1}{2}(G_V + G_R) \quad (6)$$

$$Y = \frac{9BG}{3B+G},\ \nu = \frac{3B-2G}{2(3B+G)} \quad (7)$$

We applied the aforementioned equations (7) to obtain the Young's modulus (*Y*) and Poisson's ratio (*v*). The bulk modulus can be employed to estimate the strength of atom-to-atom bonding in solids. The large bulk modulus ($B > 100$ GPa) denotes a material's comparatively hard character, while the small bulk modulus ($B < 100$ GPa) denotes a material's comparatively soft character. So, the bulk modulus in this study indicates that BiOI is a soft material. The bulk and shear modulus, in particular, describe a solid's resistance to volume and shape change, respectively. BiOI's damage tolerance, machinability, and stiffness are represented by the higher *B* with lower *G*. We are not found of any theoretical work on the elastic moduli of BiOI, hence we are unable to compare our findings to any existing data. Pugh's ratio (*B/G*) and Poisson's ratio are two key factors for establishing if a material is ductile or brittle. A material with a $B/G > 1.75$ will be ductile; on the other hand, a material with a $B/G < 1.75$ will be brittle. Likewise, the material will be ductile if $v > 0.26$; else, it would be brittle. We concluded that the examined compound is brittle based on the values of the aforementioned two factors. Furthermore, Vicker's hardness of BiOI was computed employing the given expression.

One more absorbing physical factor of solids related to elastic characteristics is elastic anisotropy. Mechanical endurance, microscopic behavior, applicability under various external stresses, and degree of elastic anisotropy are all important characteristics of a solid. These can be greatly developed by determining the degree of elastic anisotropy in a substance. As a result, a clear depiction of diverse elastic anisotropic behaviors might be useful in both basic solid-state physics and applied engineering sciences for enhancing devices were mechanical characteristics and stress affect performance and dependability. The shear anisotropic components of a crystal can also be expressed using the mentioned formulas below. The Voigt and Reuss approximations are denoted by the letters V and R, respectively. A perfect isotropic nature is depicted by a zero value, but an anisotropic nature is represented by a divergence from zero.

For isotropic solids, the value of A^U is zero. The degree of elastic anisotropy is dictated by the computed A^U of BiOI, which was also confirmed by several anisotropy indicators in our earlier discussions. 3D surface constructions (3D contour plots) and their planar projections (2D contour plots) of elastic moduli were used to visually comprehend anisotropy. Figure 5 illustrates the relationship between the Young modulus (*Y*), Shear modulus (*G*), and Poisson ratio (*v*) in two and three-dimensional directions. The 3D surface construction pattern for an isotropic crystal

should be spherical; else, the crystal will be anisotropic. The degree of elastic anisotropy in solids is measured by the divergence of the spherical 3D surface. The extremely anisotropic nature of our examined material was clearly visible, which was compatible with anisotropy indices calculations.

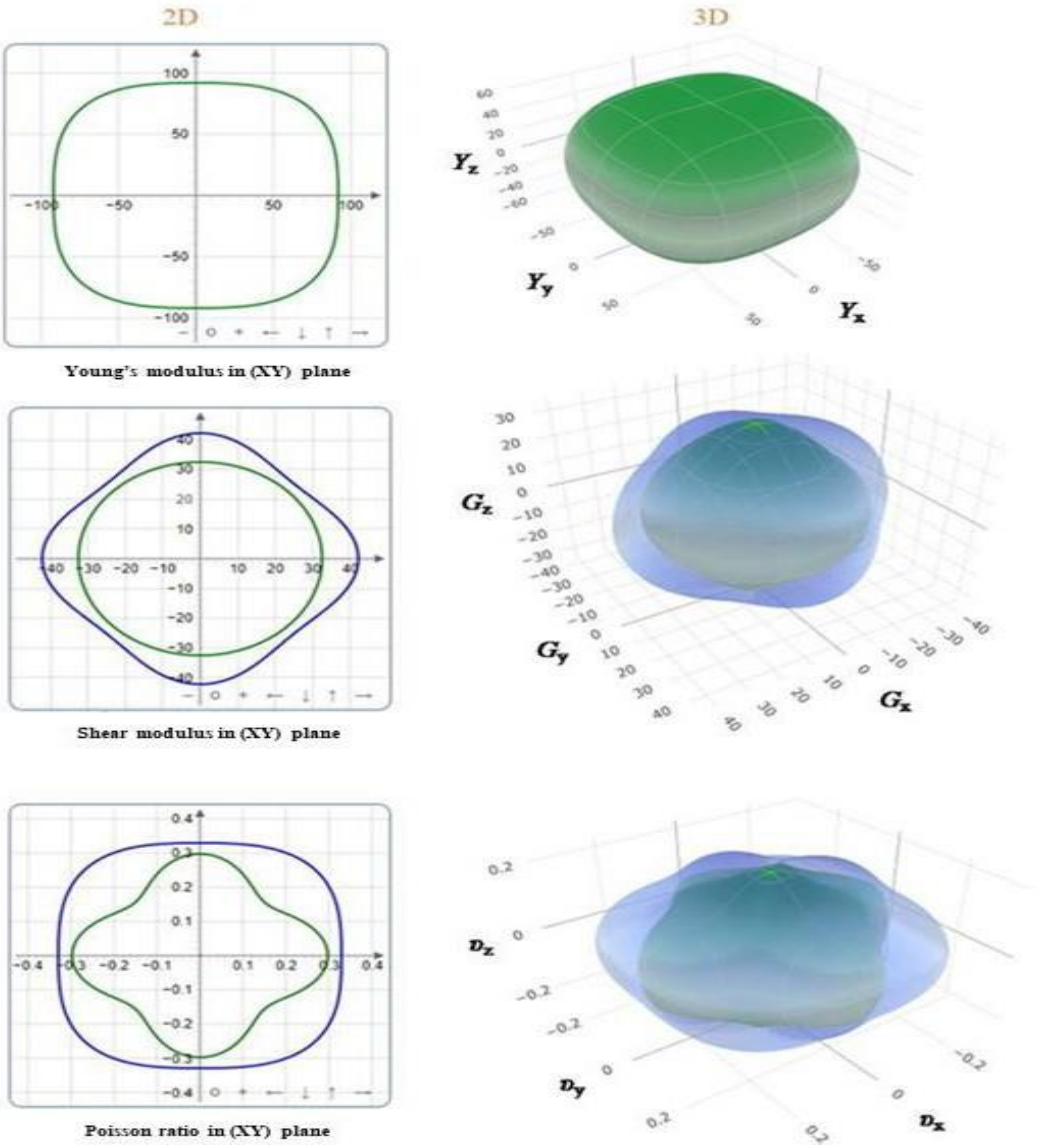

Figure 5 Anisotropy of Young's modulus, *Y* (GPa), shear modulus, *G* (GPa) and Poisson's ratio, ν in 2D (left panel) and 3D (right panel) contour plots of BiOI.

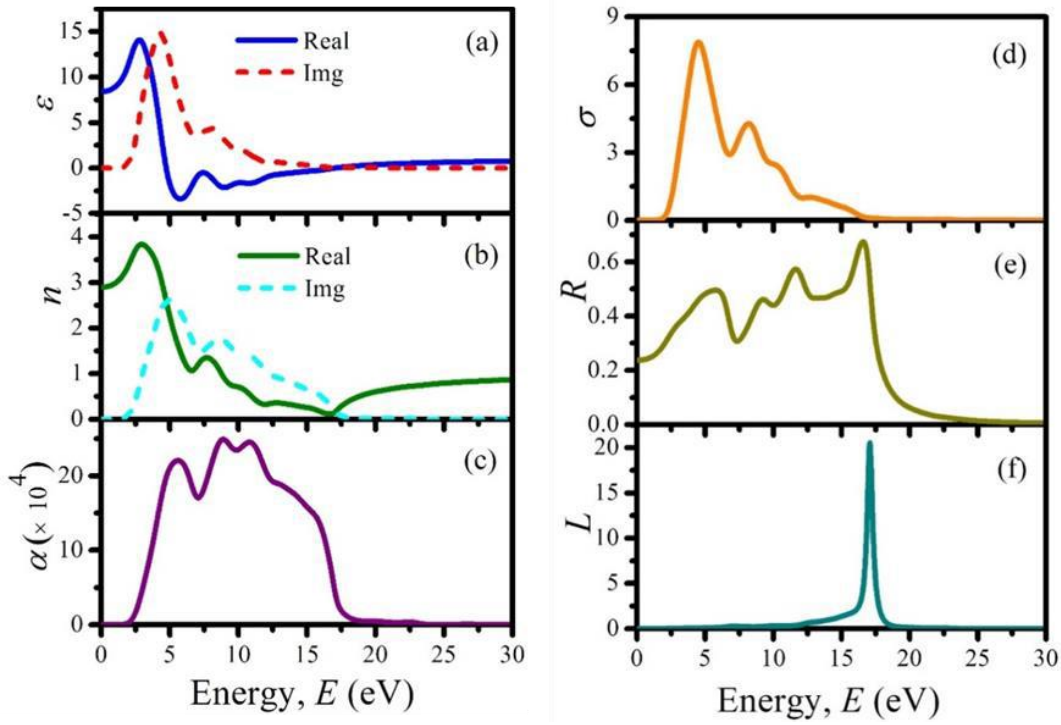

Figure 6 Energy-dependent (a) dielectric function (real and imaginary), (b) refractive index(real and imaginary), (c) absorption, (d) conductivity, (e) reflectivity, and (f) loss function of BiOI.

A number of thermal parameters, namely minimum thermal conductivity, Debye temperature (θ_D), and melting temperature (T_m), are evaluated and given in this work to better understand BiOI's thermal characteristics. Comprehending a material's behavior to an incident electromagnetic wave requires knowledge of its optical properties. As a result, these characteristics are important for investigating prospective uses in optoelectronic and photovoltaic devices. The nature of the substance in the ultraviolet, visible, and infrared spectra is extremely important for such applications. To explore the response of BiOI, distinct optical energy (frequency) dependent constraints, such as refractive index $n(\omega)$, optical conductivity $\sigma(\omega)$, loss function $L(\omega)$, dielectric constant $\varepsilon(\omega)$, absorption co-efficient $\alpha(\omega)$, and reflectivity $R(\omega)$, are estimated for photon energies up to 50 eV with electric field polarization vectors along the [100] direction; Figure 6 shows them. In general, intra-band and inter-band optical transitions are used to compute ε(ω). The indirect intra- band transition is ignored in this computation because it comprises phonons and has a smaller scattering cross-section than the direct transition, which does not require phonon scattering to conserve momentum. The real and imaginary components of the dielectric function are greater at low energy and notably diminished with rising photon energy, as seen in Figure 6(a). This behavior suggests that BiOI could be used in microelectronic devices and integrated circuits. The dielectric constant is linked to electron excitation, which is primarily caused by interband transitions with modest peaks at 7 eV caused by intraband transitions. Figure 6 (b) depicts the real and imaginary components of the refractive index. The real component declines steadily in a similar manner as real component of the dielectric function, but the imaginary component crosses the real part at ~ 5 eV and subsequently falls below the real part at ~ 17 eV. At zero photon energy, the maximal refractive index (real part) is achieved,

implying that BiOI could be used in organic light emitting diodes, quantum-dot light emitting diodes, waveguides and solar cells. The expansion seen at lower energies (~ 0 to 18 eV) owing to transitions between extremely close energy bands may be seen in the absorption spectra illustrated in Figure 6(c). The absorption coefficient of BiOI is relatively high at energy 5-12 eV, which predicts its prospective use in solar panel. Due to semiconducting nature of BiOI, the photoconductivity [Figure 6(d)] could not start at zero energy. It starts at ~ 2 eV, the maximum spectra attain at 4.51 eV, which finally becomes lower with increasing energy. The large conductivity at lower photon energy suggests the conventional applications of BiOI. Figure 6(e) presents that the zero- frequency reflectivity *R*(0) is 23% of total radiation, which is increased in the high-energy region due to the inter-band carriers. In addition, the high reflectivity (~ 67% of total radiation) at ~ 16 eV proves the potentiality BiOI to as an excellent coating element for reducing solar heating. Figure 6(f) demonstrates the energy wasted by a fast-moving electron passing through the substance. The maximum energy loss (plasma peak) occurs at ~ 17 eV, which is called the plasma frequency of BiOI. If the incident photon's energy exceeds the plasma frequency, BiOI turns translucent.

4. CONCLUSIONS

The structural, mechanical, thermal, electronic, and optical properties of tetragonal BiOI have been thoroughly examined via experimental and DFT-based first-principles calculations. The recorded XRD peaks reasonably match with the previous findings. A flaky morphology of the prepared BiOI is observed, where the flakes are perpendicularly connected with each other. The calculated lattice parameters agree well with previous reported results. Elastic constants match Born requirements, for tetragonal BiOI stability, showing that this material is mechanically stable. The brittle character of BiOI is predicted by Pugh's and Poisson's ratios. Furthermore, this compound is anisotropic nature. Because of its low Debye temperature and poor thermal conductivity, this compound can also be exploited as a thermal barrier coating material. The optical properties of BiOI have also been studied in depth, revealing a variety of potential applications, including microelectronics, organic light emitting diodes, integrated circuits, quantum-dot light emitting diodes, waveguides, solar cells, and solar heat reducing coating material.

References

[1]P. Shao, J. Tian, F. Yang, X. Duan, S. Gao, W. Shi, X. Luo, F. Cui, S. Luo, S. Wang, Adv. Funct. Mater. 28 (2018) 1705295
[2]P. Shao, Z. Ren, J. Tian, S. Gao, X. Luo, W. Shi, B. Yan, J. Li, F. Cui, Chem. Eng. J. 323 (2017) 64
[3]S. Zhang, L. Wang, C. Liu, J. Luo, J. Crittenden, X. Liu, T. Cai, J. Yuan, Y. Pei, Y. Liu, Water Res. 121 (2017) 11
[4] Ziyad Khalf Salih, Angham Ayad Kamall-Eldeen, Exp. Theo. NANOTECHNOLOGY 5 (2021) 197
[5]T. Fan, C. Chen, Z. Tang, RSC Adv. 6 (2016) 9994
[6]H. Huang, L. Liu, Y. Zhang, N. Tian, RSC Adv. 5 (2014) 1161
[7]L. Chen, D. Meng, X. Wu, A. Wang, J. Wang, M. Yu, Y. Liang, RSC Adv. 6 (2016) 52300
[8] N. Tit, N. E. Christensen, Exp. Theo. NANOTECHNOLOGY 5 (2021) 203
[9]S.M. Jain, T. Edvinsson, J.R. Durrant, Commun. Chem. 21 (2019) 1

[10] J. Xu, X. Cao, Chem. Eng. J. 260 (2015) 642